Virtual Synchronous Generator Control for Three-phase Grid-tied Inverter Using Current Source Type Electric Motor Emulator

Gensui Tanaka
Dept. of Technology of Science Innovation
Nagaoka University of Technology
Nagaoka, Japan
s203164+tanaka@stn.nagaokaut.ac.jp

Hiroki Watanabe
Dept. of Electrical, Electronics, and Information Engineering
Nagaoka University of Technology
Nagaoka, Japan
hwatanabe@vos.nagaokaut.ac.jp

Jun-ichi Itoh
Dept. of Technology of Science Innovation
Nagaoka University of Technology
Nagaoka, Japan
itoh@vos.nagaokaut.ac.jp

***Abstract*—This paper proposes a novel virtual synchronous generator (VSG) control method for a three-phase grid-tied inverter employing a current-source type electric motor emulator (EME). The proposed method enables both grid-following (GFL) and grid-forming (GFM) operations while accurately incorporating the transient dynamics of a synchronous generator's armature. By utilizing the current-source-type EME, the volume of the grid-tied inductor can be reduced, similarly to conventional current-controlled VSG approaches. Furthermore, substituting virtual impedance with a motor model not only provides virtual inertia but also enables GFM operation, which conventional current-controlled VSG schemes cannot achieve. The effectiveness of the proposed method in delivering inertia support and enabling GFM operation is demonstrated through simulation results.**

Keywords— grid-tied inverter, three-phase inverter, virtual synchronous generator, electric motor emulator

I. Introduction

Grid-tied inverters are widely used to integrate renewable energy sources, such as solar and wind power, into the utility grid. As the penetration of inverters increases, the share of conventional synchronous generators decreases, resulting in reduced grid inertia. Low grid inertia leads to significant frequency deviations during supply–demand imbalances, posing a critical challenge for the large-scale deployment of renewable energy. To address this issue, virtual synchronous generator (VSG) control has been proposed [1]–[7]. VSG control enables inverters to emulate the inertia of synchronous generators by employing the swing equation. In other words, implementing VSG control allows a grid-tied inverter to exhibit virtual inertia, similar to that of a synchronous generator. Notably, grid-tied inverters using voltage-based VSG control can operate in grid-forming (GFM) mode and contribute to grid voltage regulation.

In addition, the increasing adoption of grid-tied inverters requires system miniaturization [8], [9]. Among system components, the grid-tied inductor occupies a significant portion of the total volume. To address this, current-controlled VSG schemes have been proposed, which provide virtual inertia while reducing the size of the grid-tied inductor [10]–[13]. These methods use the swing equation to emulate virtual inertia and incorporate virtual impedance control to reduce the required inductance. However, because they rely on approximate impedance models, the transient current response is not fully accounted for. Furthermore, current-controlled VSG inverters operate in grid-following (GFL) mode and therefore cannot form grid voltage.

Meanwhile, electric motor emulators (EMEs), which replicate motor behavior using power conversion circuits, have attracted increasing attention in motor drive system development [14]–[16]. EMEs are typically classified into two types: voltage-source type and current-source type. The former emulates the back electromotive force (EMF) of the target motor while the latter replicates the motor current. Based on this classification, VSG control using a voltage-source type EME has been proposed to emulate voltage sources such as aircraft generators and synchronous machines. This approach enables both the emulation of synchronous generator dynamics, including transient behavior, and GFM operation. However, it does not support the downsizing of the interconnecting inductor.

This paper proposes a novel VSG control method for a three-phase grid-tied inverter based on a current-source-type EME. The key advantage of the proposed method is its ability to support both GFL and GFM operations while accurately capturing the transient behavior of a synchronous generator. By employing a current-source-type EME, the method allows for downsizing of the grid-tied inductor, similar to conventional current-controlled VSG approaches. Moreover, replacing the virtual impedance with a motor model not only provides virtual inertia but also enables GFM operation, which is not achievable with conventional current-controlled VSG methods. The effectiveness of the proposed control scheme in providing inertia support and enabling GFM operation is validated through simulation.

II. Current-Source Type Electric Motor Emulator

Fig. 1 illustrates the configuration of the inverter test system employing a current-source-type electric motor emulator (EME). The hardware consists of coupling inductors and a three-phase AC/DC converter, while the controller includes a motor model, current control, and pulse-width modulation (PWM). The current-source-type EME computes the motor current from the output voltage of the inverter under test (IUT). The motor behavior is emulated by regulating the current to follow the calculated reference motor current. In addition, motor torque and rotor speed are simultaneously calculated within the controller. The motor model, represented by the state-space equations of the target motor, is implemented in the controller. The state-space model of a surface permanent magnet synchronous motor (SPMSM) in the dq-axis reference frame is given by

$$p\begin{bmatrix} i_{\mathrm{d}} \\ i_{\mathrm{q}} \end{bmatrix} = \begin{bmatrix} -\dfrac{R}{L} & \omega_{\mathrm{re}} \\ -\omega_{\mathrm{re}} & -\dfrac{R}{L} \end{bmatrix} \begin{bmatrix} i_{\mathrm{d}} \\ i_{\mathrm{q}} \end{bmatrix} + \frac{1}{L}\begin{bmatrix} v_{\mathrm{d}} \\ v_{\mathrm{q}} \end{bmatrix} + \begin{bmatrix} 0 \\ -\dfrac{\omega_{\mathrm{re}}\psi}{L} \end{bmatrix}, \quad (1)$$

where i_{dq} is the dq-axis current, v_{dq} is the dq-axis stator voltage, R is the armature winding resistance, L is the armature self-inductance, ω_{re} is the electrical angular velocity of the rotor, ψ is the permanent magnet flux linkage, and p denotes the differential operator.

The relationships between output torque and electrical angular velocity are expressed in

$$T_{\mathrm{out}} = P_{\mathrm{f}}\psi i_{\mathrm{q}}, \quad (2)$$

$$p\omega_{\mathrm{re}} = \frac{P_{\mathrm{f}}}{J}(T_{\mathrm{out}} - T_{\mathrm{L}}) - P_{\mathrm{f}} D\omega_{\mathrm{re}}, \quad (3)$$

respectively, where T_{out} is the electromagnetic output torque, T_{L} is the load torque, P_{f} is the number of pole pairs, J is the moment of inertia, and D is the viscous damping coefficient.

III. Grid-connected Control Using Current-Source Type Electric Motor Emulator

A. VSG Control Using a Current-Source-Type EME

Fig. 2 shows the circuit diagram of the three-phase grid-tied inverter, and Fig. 3 illustrates the block diagram of the proposed VSG control. In this method, the IUT shown in Fig. 1 is replaced by the grid. The measured grid voltage is input into the VSG model, which calculates the corresponding VSG current. The permanent magnet flux linkage is replaced as shown in

$$\psi_{\mathrm{VSG}} = \frac{V_{\mathrm{VSG}}^{*}}{\omega_{\mathrm{grid}}}, \quad (4)$$

where ψ_{VSG} is the flux of the VSG, and V_{VSG}^{*} is the output voltage command of the VSG.

In the proposed control method, the output voltage is regulated by adjusting the VSG flux, similar to the operation of a synchronous generator. To suppress reactive power, the amplitude of the inverter output voltage vector must match the magnitude of the grid voltage vector. Therefore, the detected RMS value of the grid voltage is used as the VSG output voltage command. When the three-phase grid voltage is balanced, the RMS value is calculated from the phase voltage as shown in

$$V_{\mathrm{grid\_det}} = \sqrt{-2(v_{\mathrm{a}}v_{\mathrm{b}} + v_{\mathrm{b}}v_{\mathrm{c}} + v_{\mathrm{c}}v_{\mathrm{a}})}, \quad (5)$$

where $V_{\mathrm{grid\_det}}$ is the detected RMS value of the grid voltage, and v_{uvw} represents the instantaneous phase voltage.

Based on the above, equations (1) to (3) are reformulated as (4) to (6), assuming a pole pair number of one:

$$p\begin{bmatrix} i_{\mathrm{d}} \\ i_{\mathrm{q}} \end{bmatrix} = \begin{bmatrix} -\dfrac{R_{\mathrm{V}}}{L_{\mathrm{V}}} & \omega_{\mathrm{VSG}} \\ -\omega_{\mathrm{VSG}} & -\dfrac{R_{\mathrm{V}}}{L_{\mathrm{V}}} \end{bmatrix} \begin{bmatrix} i_{\mathrm{d}} \\ i_{\mathrm{q}} \end{bmatrix} + \frac{1}{L_{\mathrm{V}}}\begin{bmatrix} v_{\mathrm{d}} \\ v_{\mathrm{q}} \end{bmatrix} + \begin{bmatrix} 0 \\ -\dfrac{\omega_{\mathrm{VSG}}\psi_{\mathrm{V}}}{L_{\mathrm{V}}} \end{bmatrix}, \quad (6)$$

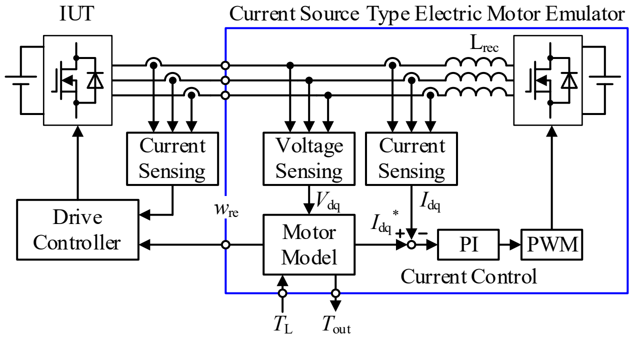

Fig. 1. Configuration of an inverter test system using the current source type electric motor emulator. Imitation of motor behavior is achieved by current control according to the current command calculated from the motor model.

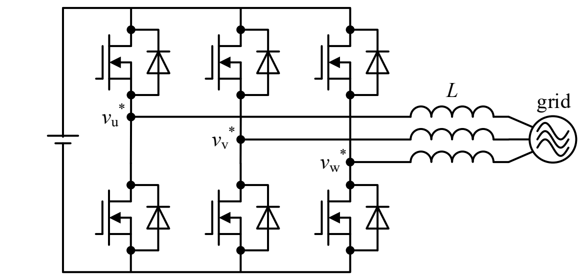

Fig. 2. Three-phase grid-tied inverter. The circuit configuration is the same as that of EME. Thus, there is no need to change the control configuration of the EME.

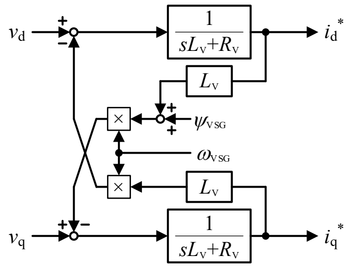

(a) VSG model.

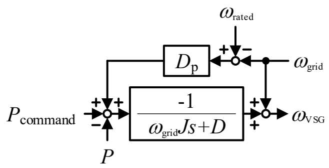

(b) Active power control with frequency droop control.

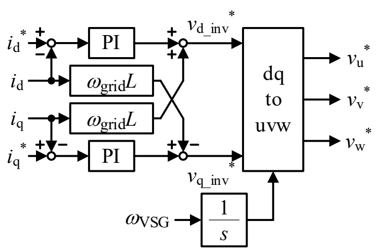

(c) Current control and PWM modulation.

Fig. 3. Block diagram of proposed VSG control. The most significant difference from the conventional method is using a VSG model that includes transient terms.

$$T_{\mathrm{VSG}} = \psi_{\mathrm{VSG}} i_{\mathrm{q}} , \tag{7}$$

$$p\omega_{\mathrm{VSG}} = \frac{1}{J_{\mathrm{V}}} (T_{\mathrm{VSG}} - T_{\mathrm{command}}) - D_{\mathrm{V}} \omega_{\mathrm{VSG}} , \tag{8}$$

where R_{V} is the virtual wiring resistance, L_{V} is the virtual interconnection inductance, ω_{VSG} is the rotational angular frequency of the VSG, T_{VSG} is the output torque of the VSG, J_{V} is the virtual moment of inertia, D_{V} is the virtual viscous damping coefficient, and ψ_{V} is the virtual flux linkage.

B. Design of Active Power Control

Fig. 4 shows a block diagram of the active power control scheme. The following assumptions are made in the control design.

(i) The load angle δ is sufficiently small,

(ii) The electrical time constant is significantly slower than the power response,

(iii) The cross-coupling effect between the dq axes is negligible,

(iv) The magnitudes of the inverter output voltage and grid voltage vectors are approximately equal.

The active power response of the system is given in

$$\frac{P_{\mathrm{out}}(s)}{P_{\mathrm{cmd}}(s)} = \frac{\dfrac{V_{\mathrm{grid}}^{2}}{J_{\mathrm{v}} \omega_{\mathrm{g}} \sqrt{\omega_{\mathrm{grid}}^{2} L_{\mathrm{v}}^{2} + R_{\mathrm{v}}^{2}}}}{s^{2} + \dfrac{D_{\mathrm{v}}}{J_{\mathrm{v}} \omega_{\mathrm{grid}}} s + \dfrac{V_{\mathrm{g}}^{2}}{J_{\mathrm{v}} \omega_{\mathrm{grid}} \sqrt{\omega_{\mathrm{grid}}^{2} L_{\mathrm{v}}^{2} + R_{\mathrm{v}}^{2}}}} , \tag{9}$$

where ω_{grid} is the grid angular frequency.

This response is designed by comparing (9) to the standard form of a second-order system, given in

$$G(s) = \frac{\omega_{\mathrm{VSG}}^{2}}{s^{2} + 2\zeta \omega_{\mathrm{VSG}} s + \omega_{\mathrm{VSG}}^{2}} , \tag{10}$$

where ω_{vsg} is the response angular frequency of the VSG control, and ζ is the damping factor of the VSG control.

From this comparison, the virtual moment of inertia and virtual damping coefficient can be derived as shown in

$$J_{\mathrm{v}} = \frac{V_{\mathrm{grid}}^{2}}{\omega_{\mathrm{vsg}}^{2} \omega_{\mathrm{grid}} \sqrt{\omega_{\mathrm{grid}}^{2} L_{\mathrm{v}}^{2} + R_{\mathrm{v}}^{2}}} , \tag{11}$$

$$D_{\mathrm{v}} = 2\zeta \omega_{\mathrm{vsg}} \omega_{\mathrm{grid}} J_{\mathrm{v}} , \tag{12}$$

respectively. In the proposed method, the active power control response is tuned based on the desired response frequency and damping factor as defined in (11) and (12).

Synchronous generators use governor control to maintain system frequency stability by adjusting output power in response to frequency deviations due to load fluctuations. For example, if the frequency decreases because of increased load, the generator raises its power output. Following this principle, frequency droop control is applied in this study as illustrated in Fig. 4(b). The deviation between the specified angular frequency and the grid frequency is multiplied by a droop coefficient and added to the active power command.

C. Grid-Forming Operation

Fig. 5 presents the block diagram of the virtual flux control scheme. Synchronous generators regulate their output voltage by adjusting magnetic flux. Similarly, the proposed method controls the inverter output voltage by manipulating virtual magnetic flux. When the system is disconnected from the grid, the grid voltage and inverter angular frequency are replaced by their respective reference values. Additionally, the inverter output voltage is regulated to match the nominal system voltage. As shown in Fig. 5, the deviation between the detected and nominal voltages is multiplied by a droop gain D_{q} and passed through an integrator with gain K_{q}. The output of the integrator is then added to the nominal voltage to generate the output voltage command.

IV. Simulation Result

Table 1 summarizes the simulation conditions. As the synchronous reactance of synchronous generators is generally greater than 50%, the virtual interconnecting inductor is set to 10.6 mH to yield a synchronous reactance of 50%. In contrast, the synchronous inductor is set to 106 μH to achieve a synchronous reactance of 0.5%. This demonstrates that the actual interconnecting inductor can be downsized in the proposed method. In practice, the design should consider volume constraints, including switching ripple and filtering requirements, which will be addressed in future work. In addition, the virtual resistance is set to 10 Ω in order to prevent fluctuations in GFM operation. Note that increasing the virtual

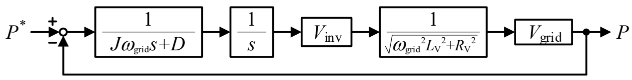

Fig. 4. The block diagram of the second-order approximated response of the output active power with the VSG control.

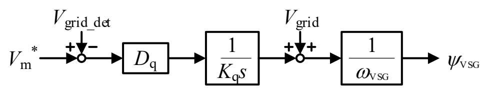

Fig. 5. Block diagram of virtual linkage flux control for GFM operation.

Table 1. Simulation conditions. The proposed method decreases the grid-tied inductance due to current control.

Parameter	Symbol	Value
Rated power	P	2 kW
Grid voltage	V_{grid}	200 V_{RMS}
Grid frequency	f_{grid}	50 Hz
Virtual inductance	L_{v}	10.6 mH (%X_{L}=50%)
Grid-tied inductance	L	1.73 μH (%X_{L}=0.5%)
Virtual resistance	R_{V}	1 Ω
Active power response frequency	f_{n}	10 Hz
Proportional gain of active power droop	D_{P}	0.1
Proportional gain of active power droop	D_{q}	-10
Damping factor	ζ	0.707
ACR bandwidth	f_{ACR}	1000 Hz

resistance excludes the assumed condition in order to design the active power response.

Fig. 6 shows the output power response when the power command is stepwise varied from 0 W to 1000 W. Note that the virtual resistance is set to 1 Ω. The active power response of the proposed method closely matches that of the second-order standard form, as illustrated in Fig. 6. Therefore, the design of the response for the reference of the active power is achieved using (11) and (12).

Fig. 7 shows the active power response when the RMS value of the grid voltage is stepwise reduced from 200 V to 160 V. As the grid voltage decreases, the active power and the VSG angular frequency also decrease accordingly. However, both the active power and the VSG angular frequency are restored by the proposed control method. These results confirm that the proposed method provides inertial support.

Fig. 8 shows the active power response when the grid frequency is stepwise decreased from 50 Hz to 48 Hz. The VSG angular frequency follows the variation in the grid frequency, demonstrating that the proposed method provides virtual inertia. Additionally, the output active power increases by 400 W as the grid frequency decreases. This response is consistent with the expected increase in active power based on the configured droop coefficient. Therefore, the implementation of frequency droop control contributes to grid stabilization by increasing output power in response to frequency decreases caused by load increases, as is the case with synchronous generators.

Fig. 9 shows the active power response during GFM operation. As shown in (a), the proposed method operates correctly even when the load is connected without a grid connection. Moreover, the voltage amplitude is maintained despite sudden changes in voltage due to load fluctuations. Although the system voltage temporarily increases during load fluctuations, it is returned to the nominal value by virtual flux control, as described in Fig. 5. As shown in (b), when the grid is disconnected, the active power varies with the load. Additionally, a transient surge occurs during the switching process. This surge depends on the load during GFM operation. Surge voltage is larger at smaller loads after switching. However, the grid voltage is maintained even in the GFM condition.

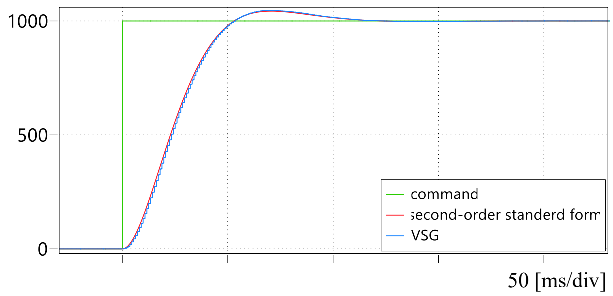

Fig. 6. Active power response.

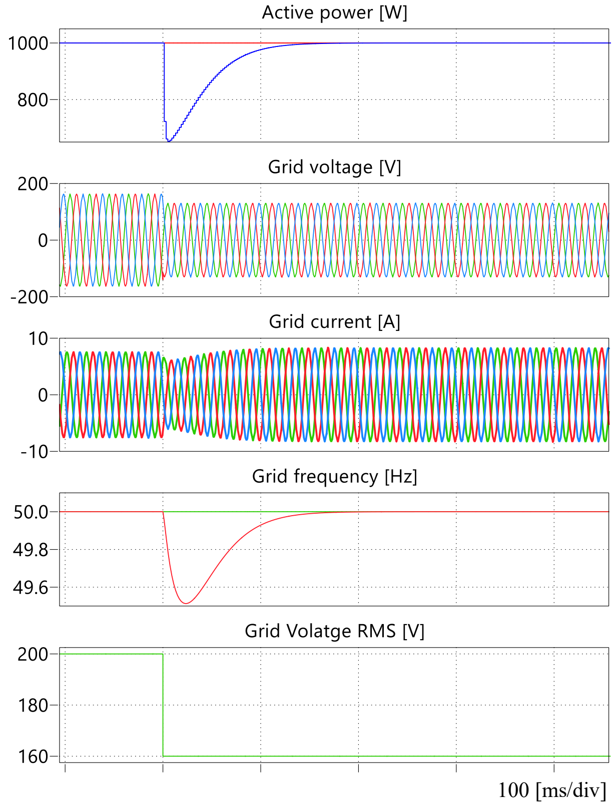

Fig. 7. Response to grid voltage fluctuation.

V. Conclusion

This paper proposed a novel VSG control method. The proposed method realizes VSG control using a current-source type EME. It enables both GFL and GFM operations while also reducing the size of the interconnecting inductor, which typically contributes to increased system volume. Simulation results confirm that the active power response follows the designed specifications. It is also verified that virtual inertia is provided in response to fluctuations in system voltage and frequency. Furthermore, it is demonstrated that the system voltage is maintained and active power is supplied to the load even under islanded conditions.

References

[1] X. Xiong, C. Wu and F. Blaabjerg, "An Improved Synchronization Stability Method of Virtual Synchronous Generators Based on Frequency Feedforward on Reactive Power Control Loop," in IEEE Transactions on Power Electronics, vol. 36, no. 8, pp. 9136-9148, Aug. 2021.

[2] Z. Shuai, C. Shen, X. Liu, Z. Li and Z. J. Shen, "Transient Angle Stability of Virtual Synchronous Generators Using Lyapunov's Direct Method," in IEEE Transactions on Smart Grid, vol. 10, no. 4, pp. 4648-4661, July 2019.

[3] H. Cheng, Z. Shuai, C. Shen, X. Liu, Z. Li and Z. J. Shen, "Transient Angle Stability of Paralleled Synchronous and Virtual Synchronous Generators in Islanded Microgrids," in IEEE Transactions on Power Electronics, vol. 35, no. 8, pp. 8751-8765, Aug. 2020.

[4] C. Li, Y. Yang, Y. Cao, A. Aleshina, J. Xu and F. Blaabjerg, "Grid Inertia and Damping Support Enabled by Proposed Virtual Inductance Control for Grid-Forming Virtual Synchronous Generator," in IEEE Transactions on Power Electronics, vol. 38, no. 1, pp. 294-303, Jan. 2023.

[5] O. Mo, S. D'Arco and J. A. Suul, "Evaluation of Virtual Synchronous Machines With Dynamic or Quasi-Stationary Machine Models," in IEEE Transactions on Industrial Electronics, vol. 64, no. 7, pp. 5952-5962, July 2017.

[6] Hirofumi Uemura, Sachio Takano, Atsushi Harada, Takahiro Matsuura, Satoshi Miyazaki, Hiromu Hamada, and Teru Miyazaki, "Emulated Inertia Control of Grid-connected Inverter-based Power Supply Sources for Mass Integration of Renewable Energy Resources," IEEJ Journal of Industry Applications, vol. 12, no. 3, pp. 368-375, 2023.

[7] Mohd. Brado Frasetyo, Fransisco Danang Wijaya, and Husni Rois Ali, "Islanded Wind Farm Microgrid Stability Control using Synchronverter Algorithm," IEEJ Journal of Industry Applications, vol. 12, no. 4, pp. 603-612, 2023.

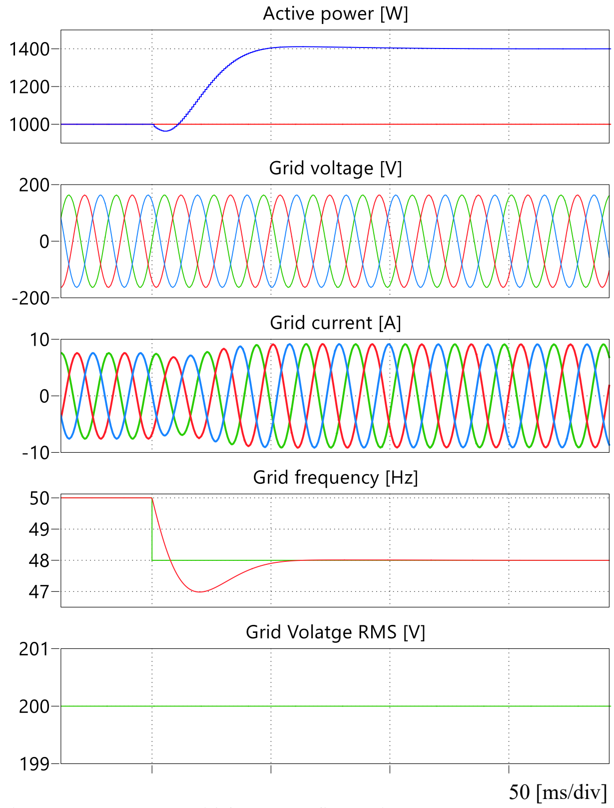

Fig. 8. Response to grid frequency fluctuation.

[8] R. Peña-Alzola, M. Liserre, F. Blaabjerg, M. Ordonez and Y. Yang, "LCL-Filter Design for Robust Active Damping in Grid-Connected Converters," in IEEE Transactions on Industrial Informatics, vol. 10, no. 4, pp. 2192-2203, Nov. 2014.

[9] S. Nagai and J. Itoh, "FRT Capability of Three-phase Grid-tied Converter with Minimized Inductor," 2019 IEEE Applied Power Electronics Conference and Exposition (APEC), Anaheim, CA, USA, 2019, pp. 1070-1077.

[10] X. Fu, M. Huang, C. K. Tse, J. Yang, Y. Ling and X. Zha, "Synchronization Stability of Grid-Following VSC Considering Interactions of Inner Current Loop and Parallel-Connected Converters," in IEEE Transactions on Smart Grid, vol. 14, no. 6, pp. 4230-4241, Nov. 2023.

[11] C. Blanco, D. Reigosa, J. C. Vasquez, J. M. Guerrero and F. Briz, "Virtual Admittance Loop for Voltage Harmonic Compensation in Microgrids," in IEEE Transactions on Industry Applications, vol. 52, no. 4, pp. 3348-3356, July-Aug. 2016.

[12] Z. Zhang, Y. Liu and J. Li, "A HESM-Based Variable Frequency AC Starter-Generator System for Aircraft Applications," in IEEE Transactions on Energy Conversion, vol. 33, no. 4, pp. 1998-2006, Dec. 2018.

[13] Kazuki Nakamura, Kaya Kawashima, Ryoko Kato, Kohsuke Seki, Kenta Yamabe, Kantaro Yoshimoto, and Tomoki Yokoyama, "Verification of 1 MHz Multisampling Disturbance Compensation Deadbeat Control for Megawatt-Level Grid-Tied Multi-level Inverter using Hardware-in-the-loop Controller," IEEJ Journal of Industry Applications, vol. 12, no. 3, pp. 427-433, 2023.

[14] R. . Kaarthik, K. S. Amitkumar and P. Pillay, "Emulation of a PermanentMagnet Synchronous Generator in Real-Time Using Power Hardware-in-the-Loop," in IEEE Transactions on Transportation Electrification, vol. 4, no. 2, pp. 474-482, June 2018.

[15] Y. Xie, J. Zhang, D. Jiang, Z. Liu and L. Tian, "Emulation of Integrated Starter/Generator Using Power Electronic Devices," in IEEE Transactions on Industry Applications, vol. 59, no. 5, pp. 6556-6567, Sept.-Oct. 2023.

[16] Q. -C. Zhong and G. Weiss, "Synchronverters: Inverters That Mimic Synchronous Generators," in IEEE Transactions on Industrial Electronics, vol. 58, no. 4, pp. 1259-1267, April 2011.

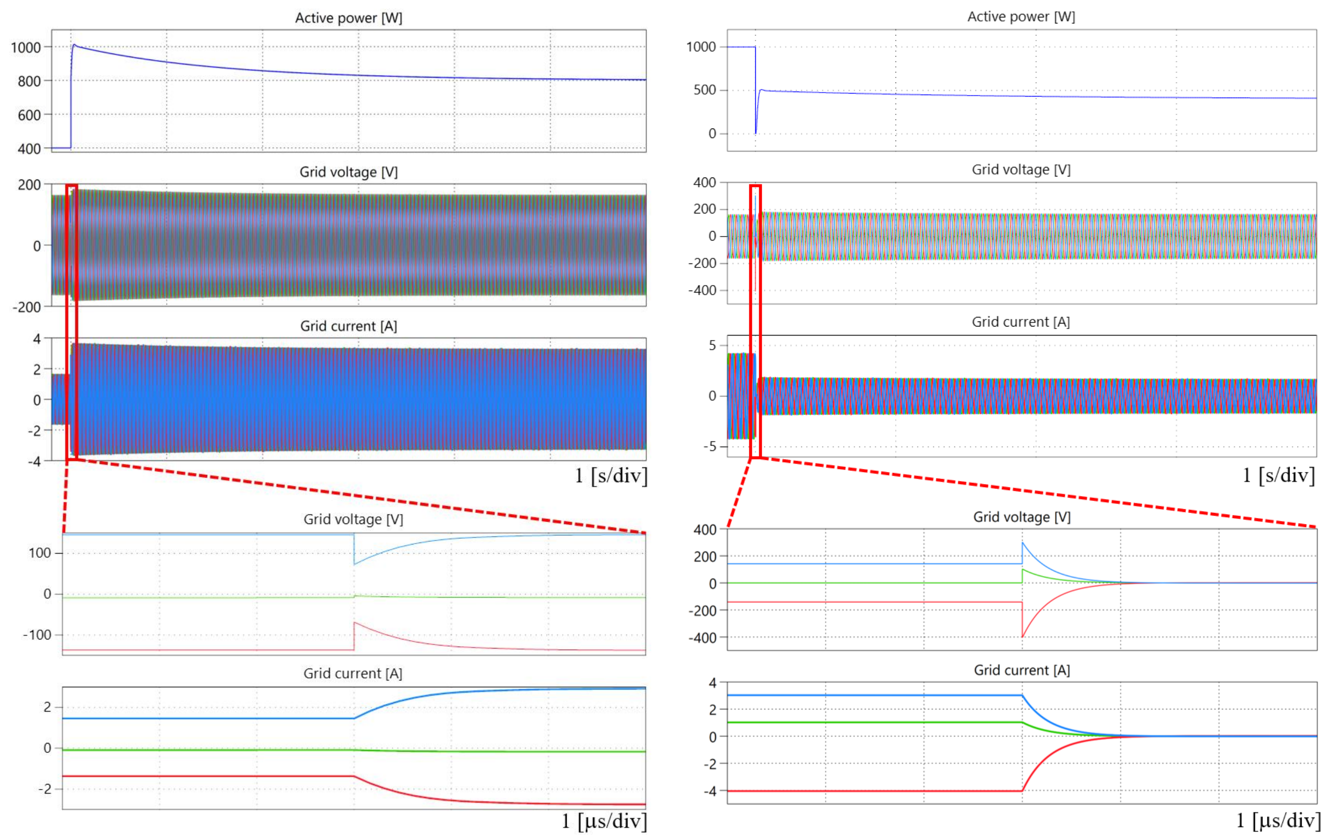

(a) Load change from 400 W to 800 W.

(b) Operation change from GFL to GFM.

Fig. 9. Waveform in GFM operation. The proposed method provides GFM operation to maintain the grid voltage when the output is connected to the load rather than the grid.